On the Cooling-to-Space Approximation

NADIR JEEVANJEE[a] AND STEPHAN FUEGLISTALER

Department of Geosciences, Princeton University, Princeton, New Jersey

(Manuscript received 7 December 2018, in final form 15 August 2019)

ABSTRACT

The cooling-to-space (CTS) approximation says that the radiative cooling of an atmospheric layer is dominated by that layer's emission to space, while radiative exchange with layers above and below largely cancel. Though the CTS approximation has been demonstrated empirically and is thus fairly well accepted, a theoretical justification is lacking. Furthermore, the intuition behind the CTS approximation cannot be universally valid, as the CTS approximation fails in the case of pure radiative equilibrium. Motivated by this, we investigate the CTS approximation in detail. We frame the CTS approximation in terms of a novel decomposition of radiative flux divergence, which better captures the cancellation of exchange terms. We also derive validity criteria for the CTS approximation, using simple analytical theory. We apply these criteria in the context of both gray gas pure radiative equilibrium (PRE) and radiative–convective equilibrium (RCE) to understand how the CTS approximation arises and why it fails in PRE. When applied to realistic gases in RCE, these criteria predict that the CTS approximation should hold well for H_2O but less so for CO_2, a conclusion we verify with line-by-line radiative transfer calculations. Along the way we also discuss the well-known "$\tau = 1$ law," and its dependence on the choice of vertical coordinate.

1. Introduction

The cooling-to-space approximation is a venerable tool of radiative transfer. Formulated over 50 years ago (M. Zagoni 2016, unpublished manuscript; Green 1967; Rodgers and Walshaw 1966), it gives a simplified description of radiative cooling suitable for textbooks (Wallace and Hobbs 2006; Petty 2006; Thomas and Stamnes 2002), heuristics and idealized modeling (Jeevanjee and Fueglistaler 2020; Jeevanjee and Romps 2018), and has served in the past as a basis for comprehensive radiation schemes (Eymet et al. 2004; Joseph et al. 1976; Fels and Schwarzkopf 1975; Rodgers and Walshaw 1966). Its content is simply that radiative cooling in a given layer can be approximated as that layer's emission or cooling to space (CTS), as radiative exchange between atmospheric layers can be neglected. This claim is quite intuitive, as the exchange terms are sourced by the temperature *difference* between layers, whereas the CTS term is sourced by the absolute temperature of a layer. Furthermore, exchange with cooler layers above offsets exchange with warmer layers below. This "double cancellation" in the sum of exchange terms should render that sum negligible.

This logic is plausible, and the CTS approximation indeed seems to hold quite well for terrestrial atmospheric profiles (e.g., Clough et al. 1992; Rodgers and Walshaw 1966; Fig. 6 below). However, to our knowledge a formal justification has never been given. We thus have no precise understanding of why the CTS approximation works in Earth's atmosphere, or under what conditions it might fail (on Earth or elsewhere). Furthermore, it is clear that the CTS approximation *does* fail in some cases, such as the textbook case of a gray gas in pure radiative equilibrium (PRE; e.g., Pierrehumbert 2010). This state has zero radiative cooling by definition, and thus the CTS term must be entirely canceled by the exchange terms. We are thus led to the following questions:

1) Under what conditions does the CTS approximation hold?
2) How do these conditions break down (as they must in PRE), and how can this be reconciled with the double cancellation argument given above?

The goal of this paper is to shed light on these questions. A key ingredient in our analysis will be a refinement of the canonical decomposition of radiative flux divergence given by Green (1967) into a new decomposition which naturally captures the double cancellation described above, and which also isolates the contributions which do not

[a] Current affiliation: Program in Atmosphere and Ocean Sciences, Princeton University, Princeton, New Jersey.

Corresponding author: Nadir Jeevanjee, nadirj@princeton.edu

DOI: 10.1175/JAS-D-18-0352.1

cancel (section 2). We apply this framework to gray PRE, to understand how the CTS approximation can break down (section 3). In sections 4 and 5 we then turn to gray gas radiative–convective equilibrium (RCE), to understand how the CTS approximation emerges, along with its concomitant "$\tau = 1$ law" (Huang and Shahabadi 2014). Finally in section 6 we consider cooling from realistic greenhouse gases, using the line-by-line Reference Forward Model (Dudhia 2017). Along the way we construct validity criteria for the CTS approximation capable of explaining its breakdown for the PRE state as well as its success for H_2O in RCE, and which also correctly predicts that the CTS approximation should hold only marginally for CO_2 in RCE. We also consider the impact of the choice of vertical coordinate on the CTS approximation and the $\tau = 1$ law. We do not consider radiative heating by solar absorption, though this is formally very similar to the CTS term (e.g., Jeevanjee and Romps 2018), so any results concerning the CTS term also apply to solar absorption.

2. A new decomposition of radiative flux divergence

a. Derivation

We begin by constructing a new decomposition of radiative flux divergence. For clarity and simplicity we do this first for a two-stream gray gas using optical depth τ as the vertical coordinate, extending our analysis later to realistic gases and the more conventional pressure coordinate.

The new decomposition we pursue is in some sense a refinement of the standard decomposition of radiative flux divergence found in textbooks, which says that radiative cooling in a given atmospheric layer can be decomposed into that layer's cooling to space, as well as its radiative exchange with layers above and below as well as the ground. Formally this can be expressed as (e.g., Petty 2006; Thomas and Stamnes 2002; Green 1967; Rodgers and Walshaw 1966):

$$\frac{dF}{d\tau} = [B_s - B(\tau)]\exp[-(\tau_s - \tau)] \quad \text{(GX)} \tag{1a}$$

$$- B(\tau)\exp(-\tau) \quad \text{(CTS)} \tag{1b}$$

$$+ \int_{\tau}^{\tau_s} [B(\tau') - B(\tau)]\exp[-(\tau' - \tau)]\, d\tau' \quad (\text{EX}_{\text{below}}) \tag{1c}$$

$$+ \int_{0}^{\tau} [B(\tau') - B(\tau)]\exp[-(\tau - \tau')]\, d\tau' \quad (\text{EX}_{\text{above}}). \tag{1d}$$

Here F is the net upward flux (W m^{-2}), τ_s is the surface optical depth, and B_s is the value of the source function at the surface, which may be discontinuous from the source function $B(\tau_s)$ of the atmosphere at the surface. The GX term in (1a) is the "ground exchange" term, representing exchange between level τ and the surface. The CTS term in Eq. (1b) is the product of the source function and the transmissivity $e^{-\tau}$, and thus represents the cooling to space, which is also the contribution of level τ to the outgoing longwave radiation. The CTS approximation is then just the claim that this term dominates Eq. (1), that is, that

$$\partial_\tau F \approx -B(\tau)e^{-\tau} \quad \text{(CTS approximation)}. \tag{2}$$

The EX_{below} and EX_{above} terms in Eqs. (1c) and (1d) represent radiative exchange with layers below and above. As mentioned above, these terms are generated by temperature differences, unlike the CTS term, and since temperatures change monotonically over large swaths of atmosphere (the troposphere, stratosphere, etc.), EX_{below} and EX_{above} typically have opposite signs and thus offset each other. A key point, however, is that the degree to which they cancel is in part tied to their respective ranges of integration: if $\tau_s - \tau$ is not comparable to τ, that is, if the emissivity above level τ is not comparable to that below τ, then the integrals in Eqs. (1c) and (1d) will not be comparable, inhibiting cancellation. This possibility is key for understanding how the CTS approximation can break down.

To separate out the parts of EX_{below} and EX_{above} which might cancel each other, we first change the dummy integration variable in Eqs. (1c) and (1d) to measure the optical distance from level τ, that is, we set $x \equiv \tau' - \tau$ in (1c) and $x \equiv \tau - \tau'$ in Eq. (1d). This yields

$$\text{EX}_{\text{below}} = \int_0^{\tau_s - \tau} [B(\tau + x) - B(\tau)]e^{-x}\, dx,$$

$$\text{EX}_{\text{above}} = -\int_0^{\tau} [B(\tau) - B(\tau - x)]e^{-x}\, dx.$$

The EX_{below} and EX_{above} integrals now look similar, but with potentially different limits of integration. Cancellation will most naturally occur between those parts of the integral with the same range of integration,

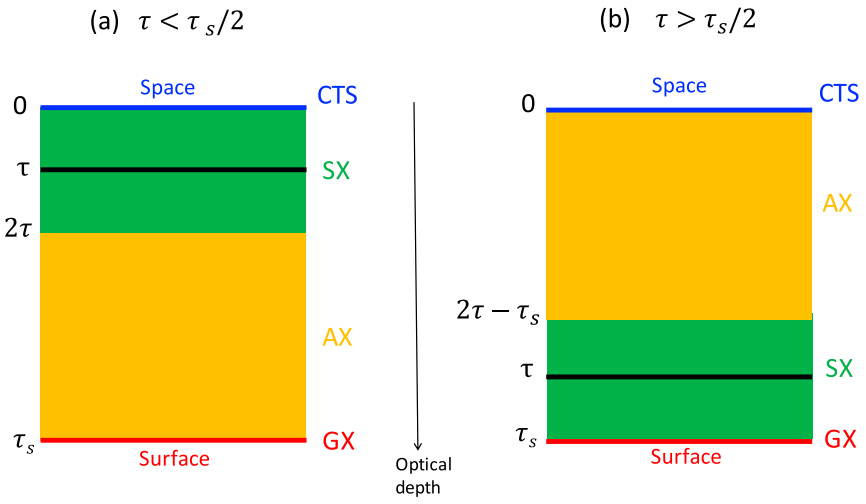

FIG. 1. Cartoon depicting the atmospheric layers relevant for the different cooling terms in Eq. (4), relative to a given layer at optical depth τ, for (a) $\tau < \tau_s/2$ and (b) $\tau > \tau_s/2$.

so we combine them. To do this we first consider the case where $\tau < \tau_s/2$ (i.e., the layer below is optically deeper than that above, Fig. 1a). In this case we split the $\mathrm{EX}_{\mathrm{below}}$ integral into an integral over the x interval $(0, \tau)$ (same as the range for the $\mathrm{EX}_{\mathrm{above}}$ integral), and an integral over the x interval $(\tau, \tau_s - \tau)$. Combining these terms with the $\mathrm{EX}_{\mathrm{above}}$ integral then gives:

$$\mathrm{EX}_{\mathrm{below}} + \mathrm{EX}_{\mathrm{above}} = \int_0^{\tau} [B(\tau + x) - 2B(\tau) + B(\tau - x)]e^{-x}\,dx \quad (\mathrm{SX}, \tau < \tau_s/2) \tag{3a}$$

$$+ \int_{\tau}^{\tau_s - \tau} [B(\tau + x) - B(\tau)]e^{-x}\,dx \quad (\mathrm{AX}, \tau < \tau_s/2). \tag{3b}$$

The integral in Eq. (3a) represents exchange between level τ and layers both above *and* below with equal optical thickness, so we refer to it as the symmetric exchange (SX) term. The integral in Eq. (3b) represents the residual, uncompensated heating from layers further below, which we refer to as the asymmetric exchange (AX) term. The regions contributing to these terms are shown schematically in Fig. 1a.

Note that the SX integrand (3a) looks like a finite-difference approximation for a second derivative; in fact, if B is linear in τ then SX vanishes, because the cooling from the layer of depth τ above exactly cancels the heating from the layer of depth τ below. This difference of differences *is* the "double cancellation" described above, and in fact occurs in gray models of pure radiative equilibrium (section 3). Furthermore, in the limit that the SX term can indeed be approximated by a second derivative, we obtain the "diffusive" approximation to radiative cooling well known from textbooks (e.g., Pierrehumbert 2010; Goody and Yung 1989; Andrews et al. 1987). Note also that it is the SX term which yields strong radiative heating and cooling at the tropopause and stratopause respectively (e.g., Clough and Iacono 1995), as B has local extrema there and thus the $\mathrm{EX}_{\mathrm{below}}$ and $\mathrm{EX}_{\mathrm{above}}$ contributions do not compensate.

Returning to the $\mathrm{EX}_{\mathrm{below}}$ and $\mathrm{EX}_{\mathrm{above}}$ terms, if instead $\tau > \tau_s/2$ we then split the $\mathrm{EX}_{\mathrm{above}}$ (rather than the $\mathrm{EX}_{\mathrm{below}}$) integral into an integral over the x intervals $(0, \tau_s - \tau)$ and $(\tau_s - \tau, \tau)$, yielding

$$\mathrm{EX}_{\mathrm{below}} + \mathrm{EX}_{\mathrm{above}} = \int_0^{\tau_s - \tau} [B(\tau + x) - 2B(\tau) + B(\tau - x)]e^{-x}\,dx \quad (\mathrm{SX}, \tau > \tau_s/2) \tag{3c}$$

$$- \int_{\tau_s - \tau}^{\tau} [B(\tau) - B(\tau - x)]e^{-x}\,dx \quad (\mathrm{AX}, \tau > \tau_s/2). \tag{3d}$$

The regions now contributing to SX and AX are shown in Fig. 1b. Note that AX now represents a cooling from layers above, rather than a heating from layers below. We will see below that this cooling leads to a failure of the CTS approximation near the surface.

These definitions of SX and AX then yield a new decomposition of radiative flux divergence, given by

$$\frac{dF}{d\tau} = \mathrm{CTS} + \mathrm{SX} + \mathrm{AX} + \mathrm{GX}. \tag{4}$$

This decomposition will be used throughout the paper.

b. Scale analysis

As a first application of Eq. (4), we make a rough scale analysis of its terms to derive an initial validity criterion for the CTS approximation. Note that the only quantities appearing so far are τ_s, B_s, and $B(\tau)$, with $B(\tau)$ the only function. Ignoring the parameters τ_s and B_s for the moment, we focus on how the properties of $B(\tau)$ might influence the CTS approximation. If we approximate all finite differences of $B(\tau)$ as derivatives, and ignore for the moment the exponential transmissivity factors as well as any integration (these will be discussed further below, particularly in appendix A), then the terms in Eq. (4) roughly scale as follows:

$$\begin{aligned} \mathrm{CTS} &\sim B, \\ \mathrm{AX}, \mathrm{GX} &\sim \frac{dB}{d\tau}, \\ \mathrm{SX} &\sim \frac{d^2B}{d\tau^2}. \end{aligned} \tag{5}$$

This shows that the CTS term is distinguished by the fact that it represents one-way exchange to space, and is thus proportional to B rather than a derivative of B. Equation (5) then suggests heuristically that the CTS approximation, Eq. (2), will hold if these derivatives of B are small compared to B itself, that is, if

$$\frac{dB}{d\tau} \ll B, \tag{6a}$$

$$\frac{d^2B}{d\tau^2} \ll B. \tag{6b}$$

This is our first validity criterion for the CTS approximation (note that this criterion was derived by ignoring the exponential transmissivity factors and integrals in the exchange terms, which will turn out to limit the criterion's validity away from $\tau \approx 1$; cf. section 5). We will apply this criterion to pure radiative equilibrium in the next section, and refine it into a more precise criterion in section 4.

3. Pure radiative equilibrium and the CTS approximation

We now apply the decompositions (1) and (4) as well as the validity criterion (6) to a gray gas in pure radiative equilibrium. We do this to provide a simplified context in which to compare decompositions, and also to better understand how the CTS approximation breaks down, resolving the paradox highlighted in question 2 from the introduction.

The two-stream gray PRE solution is written most naturally in τ coordinates, with the outgoing longwave radiation (OLR) as the sole parameter. Denoting the gray upwelling and downwelling fluxes by U and D, this solution is (Pierrehumbert 2010):

$$\begin{aligned} U &= \mathrm{OLR}\left(1 + \frac{\tau}{2}\right), \quad D = \frac{\mathrm{OLR}}{2}\tau, \\ B &= \frac{\mathrm{OLR}}{2}(1 + \tau), \quad B_s = \frac{\mathrm{OLR}}{2}(2 + \tau_s). \end{aligned} \tag{7}$$

Note that the source function at the surface B_s is discontinuous with that in the atmosphere, and is found by requiring continuity of U at the surface, $B_s = U(\tau_s)$. It is straightforward to check that the PRE solution above satisfies the PRE constraint $U + D = 2B$, which says that the (upwelling and downwelling) thermal emission per unit optical depth $2B$ is equal to the absorbed upwelling and downwelling flux per unit optical depth, $U + D$.

We now apply the old decomposition (1) to the solution (7) for $B(\tau)$, integrating where necessary to obtain analytical expressions for the various components of the flux divergence:

$$\begin{aligned} \mathrm{CTS} &= -\frac{\mathrm{OLR}}{2}(1 + \tau)e^{-\tau}, \\ \mathrm{EX}_{\mathrm{above}} &= -\frac{\mathrm{OLR}}{2}[1 - (1 + \tau)e^{-\tau}], \\ \mathrm{EX}_{\mathrm{below}} &= \frac{\mathrm{OLR}}{2}[1 - (\tau_s - \tau + 1)e^{-(\tau_s - \tau)}], \\ \mathrm{GX} &= \frac{\mathrm{OLR}}{2}(\tau_s - \tau + 1)e^{-(\tau_s - \tau)}. \end{aligned} \tag{8}$$

These terms add to 0, as they must, and are plotted for $\tau_s = 20$ in Fig. 2a. The CTS and GX terms behave equally and oppositely at their respective boundaries, with the discontinuity $B_s - B(\tau_s)$ at the surface yielding a source term jump equivalent to the jump between the atmosphere and space. The $\mathrm{EX}_{\mathrm{above}}$ and $\mathrm{EX}_{\mathrm{below}}$ terms

cancel throughout most of the atmosphere, but decline toward the boundaries as the optical thickness of the relevant exchange layers declines to 0. In this picture, the CTS term does not dominate even for $\tau \sim O(1)$ due to cancellation by $\mathrm{EX}_{\mathrm{below}}$, though $\mathrm{EX}_{\mathrm{below}}$ itself is partially canceled by $\mathrm{EX}_{\mathrm{above}}$.

A clearer picture is obtained by applying the new decomposition (4) to our PRE solution (7), which yields

$$\begin{aligned}
\mathrm{CTS} &= -\frac{\mathrm{OLR}}{2}(1+\tau)e^{-\tau},\\
\mathrm{SX} &= 0,\\
\mathrm{AX} &= \frac{\mathrm{OLR}}{2}[-(\tau_s-\tau+1)e^{-(\tau_s-\tau)}+(1+\tau)e^{-\tau}],\\
\mathrm{GX} &= \frac{\mathrm{OLR}}{2}(\tau_s-\tau+1)e^{-(\tau_s-\tau)}. \qquad (9)
\end{aligned}$$

These terms again add to 0, as they must, but now the SX term is also itself identically 0 because B is linear in τ. Each term in Eq. (9) is plotted for $\tau_s = 20$ in Fig. 2b. In the new decomposition, the nonzero cooling terms only contribute near the "boundaries" in τ space, that is, for $\tau \approx 1$ or $\tau_s - \tau \approx 1$; the residual, uncompensated exchange heating in AX is suppressed throughout the rest of the atmosphere (where τ and $\tau_s - \tau$ are large) due to the e^{-x} transmissivity factor in Eqs. (3b) and (3d). This simplicity highlights the advantages of the new decomposition. Near the boundaries, AX provides a significant heating around $\tau \sim O(1)$ and cooling around $(\tau_s - \tau) \sim O(1)$, and for PRE the B profile is such that the AX heating around $\tau \sim O(1)$ exactly cancels the CTS term, and the AX cooling around $(\tau_s - \tau) \sim O(1)$ exactly cancels GX.

Thus, we may answer question 2 from the introduction as follows: In PRE the double cancellation argument holds perfectly (i.e., SX = 0), but only to the extent that there is appreciable optical depth both above and below a given layer (which suppresses AX). This assumption is implicit in the double cancellation heuristic and can indeed hold throughout much of the atmosphere, but will fail near the boundaries, where there is indeed significant AX heating. In terms of our criteria (6), the criterion $d^2B/d\tau^2 \ll B$ holds but $dB/d\tau \ll B$ does not, as Eq. (7) shows that $dB/d\tau \sim B$, at least for $\tau \sim O(1)$ where the CTS term is significant.

4. Radiative–convective equilibrium and the CTS approximation

Having considered the simpler PRE case, we now consider a gray atmosphere in RCE, which will exhibit nonzero radiative cooling. As emphasized above and as was evident for PRE, the decomposition (4) and the validity of the CTS approximation (2) depend largely on the form of $B(\tau)$. In RCE however, the temperature (or B) profile is no longer part of the solution, but is instead given by a predetermined convective adiabat (one may take this as the definition of RCE, at least in this context). For simplicity, we take this adiabat to have a constant lapse rate Γ, so that

$$T = T_s(p/p_s)^{R_d\Gamma/g}, \qquad (10)$$

where T_s and p_s are surface temperature and pressure, respectively, and all other symbols have their usual meaning. Note that T is now continuous at the surface, so $B(\tau_s) = B_s$. To determine the form of $B(\tau)$ in RCE, we combine Eq. (10) with the commonly used power-law form for $\tau(p)$ (e.g., Cronin and Jansen 2016; Robinson and Catling 2012; Frierson et al. 2006):

$$\tau = \tau_s(p/p_s)^{\beta}. \qquad (11)$$

We also assume that

$$B(T) = B_s(T/T_s)^{\alpha} \qquad (12)$$

[$\alpha = 4$ for a gray gas, but we keep Eq. (12) general for later use]. Combining Eqs. (10)–(12), we find

$$B(\tau) = B(\tau_s)(\tau/\tau_s)^{\gamma}, \qquad (13)$$

where

$$\gamma \equiv \frac{d\ln B}{d\ln\tau} \qquad (14a)$$

$$= \underbrace{\left(\frac{d\ln B}{d\ln T}\right)}_{\substack{\text{Source}\\ \text{function}}}\underbrace{\left(\frac{d\ln T}{d\ln p}\right)}_{\substack{\text{Atmospheric}\\ \text{state}}}\underbrace{\left(\frac{d\ln\tau}{d\ln p}\right)^{-1}}_{\substack{\text{GHG}\\ \text{distribution}}} \qquad (14b)$$

$$= \alpha\frac{R_d\Gamma}{g}\frac{1}{\beta}. \qquad (14c)$$

Equation (14c) is a key result, as the parameter γ determines how rapidly thermal emission varies with optical depth and is thus critical for what follows. Furthermore, as Eq. (14b) shows, γ is a combination of multiple factors and it is worth pausing to compare and contrast them. The factor $\alpha = d\ln B/d\ln T$ in (14b) is a property of the source function only, must be externally specified, and does not depend on atmospheric state or greenhouse gas (GHG) concentrations.[1] The optical depth exponent

[1] Note that for real greenhouse gases α will depend on wavenumber; however, this consideration is not relevant for the gray case discussed here. This wavenumber dependence will be discussed in section 6b.

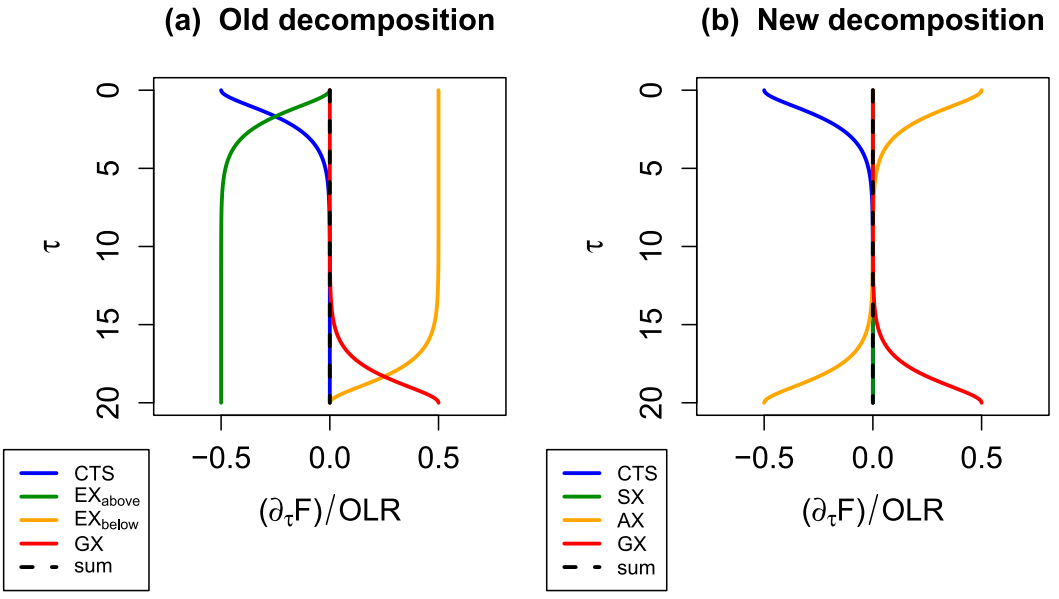

FIG. 2. (a) Old and (b) new decompositions, Eqs. (8) and (9), for the gray gas PRE solution (7) for $\tau_s = 20$. The CTS approximation (2) fails for $\tau \sim O(1)$, due to the presence of the uncompensated asymmetric exchange term AX [see (b)]. Note that the cancellation of $\mathrm{EX}_{\mathrm{above}}$ and $\mathrm{EX}_{\mathrm{below}}$ in (a) is captured implicitly by SX = 0 in (b).

$\beta = d\ln\tau/d\ln p$ indicates how "bottom heavy" the greenhouse gas and optical depth distributions are (with respect to pressure), and must also be externally specified. The lapse rate factor $d\ln T/d\ln P$ gives the atmospheric temperature profile, but whether or not it is externally specified differs between PRE and RCE. In PRE the γ profile is fixed by the solution (7) to be

$$\gamma_{\mathrm{PRE}} \equiv \frac{\tau}{1+\tau},$$

and $d\ln T/d\ln P$ then takes on whatever values are required to produce this. In contrast, in RCE it is $d\ln T/d\ln P$ which is fixed [e.g., Eq. (10)], and this then determines the γ profile [as per Eq. (14c)].

Proceeding on, we substitute Eq. (13) into the rough scalings (5) to obtain

$$\mathrm{AX}, \mathrm{GX} \sim \frac{\gamma B}{\tau}, \tag{15a}$$

$$\mathrm{SX} \sim \frac{\gamma(\gamma-1)B}{\tau^2}, \tag{15b}$$

which says that the exchange terms should be enhanced/suppressed by one or more factors of γ relative to the CTS term.[2] Indeed, a somewhat more rigorous analysis (appendix A) shows that for $\tau_s \gg 1$ and near $\tau = 1$,

$$\begin{aligned}
\mathrm{CTS}|_{\tau=1} &= -\frac{B}{e}, \\
\mathrm{SX}|_{\tau=1} &\approx \frac{\gamma(\gamma-1)}{6}B, \\
\mathrm{AX}|_{\tau=1} &\approx \frac{2\gamma}{e}B, \\
\mathrm{GX}|_{\tau=1} &\lesssim \frac{\gamma}{e}B.
\end{aligned} \tag{16}$$

Thus, the CTS approximation (2) will be satisfied if

$$\gamma \ll 1. \tag{17}$$

This is a more precise version of our first CTS criterion (6), and provides an answer to question 1 from the introduction. (Note, however, that this criterion is restricted in that it only holds for $\tau_s \gg 1$ and near $\tau = 1$.) As a first, quick test, we note that $\gamma_{\mathrm{PRE}}|_{\tau=1} = 0.5$ and thus PRE fails the criterion (17), as it should.

5. Gray RCE, pressure coordinates, and the $\tau = 1$ law

To further test Eq. (17), as well as gain insight into the transition from PRE to a CTS-dominated RCE, Figs. 3a–c shows the decomposition (4) as applied to gray PRE as well as the gray RCE profile (13) with $\gamma = 0.5$ and 0.1. (All cases have $\alpha = 4$ and $\tau_s = 20$. In PRE we set $\beta = 2$, and for RCE we set $T_s = 300\,\mathrm{K}$, $\Gamma = 7\,\mathrm{K\,km^{-1}}$, and β is

[2] Note that because these scalings are derived from the scalings in Eq. (5), the same caveats given there about limited validity away from $\tau \approx 1$ apply here.

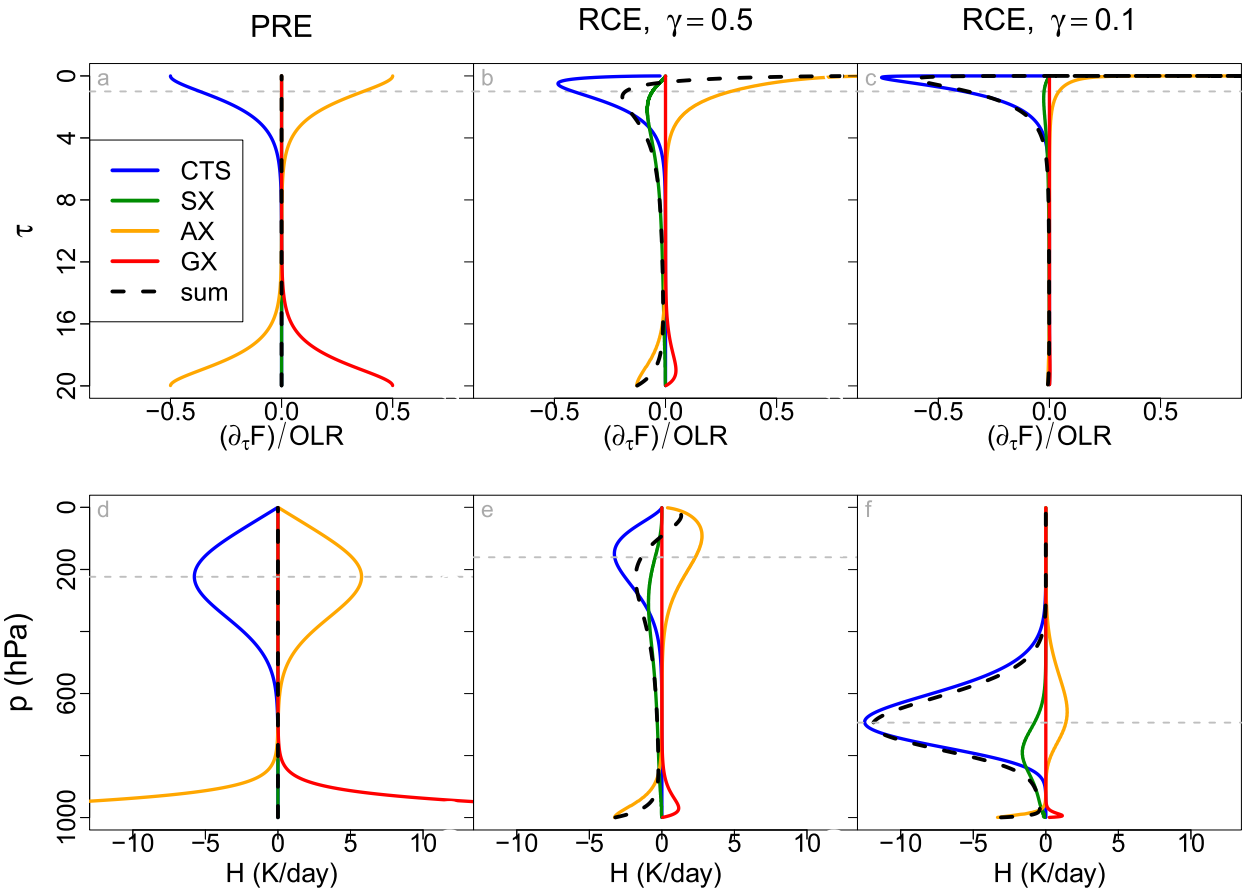

FIG. 3. (a)–(c) Decomposed and normalized $\partial_\tau F$ profiles for PRE, RCE with $\gamma = 0.5$, and RCE with $\gamma = 0.1$. In RCE the exchange terms are suppressed by factors of γ, and further suppressed near the surface by factors of $1/\tau$ [Eq. (15)]. The CTS term dominates as $\gamma \to 0$, consistent with Eq. (17). (d)–(f) As in (a)–(c), but in pressure coordinates. Surface terms are now enhanced relative to (a)–(c), and maxima emerge near $\tau = 1$ ($\tau = 1$ marked by dashed gray lines). See text for discussion.

determined by γ. The OLR in PRE is taken to be the average of the OLR from the two RCE cases.) For $\gamma = 0.5$ we find that, unlike the PRE case, AX near $\tau = 1$ is somewhat suppressed relative to CTS, due to the factor of γ in Eq. (15a), and that AX and GX are both strongly suppressed near the surface, due to both γ as well as the factor of $1/\tau$ in Eq. (15a) (which at the surface is $1/\tau_s = 1/20$). This $1/\tau$ factor is due physically to the decrease of $dB/d\tau$ with τ (because $\gamma < 1$), which suppresses the exchange terms, particularly near the surface when $\tau_s \gg 1$.

The above effects are all further enhanced for the $\gamma = 0.1$ case. Here, the exchange terms essentially disappear near the surface, and are very small at lower τ, except for the AX term for $\tau \ll 1$. In this case the CTS approximation is very good indeed, in agreement with Eq. (17).

Though Figs. 3a–c and the discussion above paint a picture for how the CTS term comes to dominate in RCE, the profiles in Figs. 3a–c do not have a familiar shape, and in particular do not obey the usual $\tau = 1$ law, according to which cooling profiles exhibit maxima at $\tau = 1$ (e.g., Huang and Shahabadi 2014; Wallace and Hobbs 2006; Petty 2006; see also appendix B). Indeed, the maxima of the CTS term (1b) for PRE [Eq. (9)] and RCE [Eq. (13)] occur at $\tau = 0$ and $\tau = \gamma$, respectively.

The resolution of this puzzle is that the profiles in Figs. 3a–c are flux divergences computed in τ coordinates, which are not the usual coordinates.[3] Usually one is instead interested in heating rates $\mathscr{H}$, which are flux divergences computed in pressure (or mass) coordinates:

$$\mathscr{H} \equiv \frac{g}{C_p}\partial_p F. \tag{18}$$

We can decompose $\mathscr{H}$ by multiplying each term in Eq. (4) by $(g/C_p)(d\tau/dp)$, yielding the profiles shown

[3] Indeed, for realistic, nongray gases the τ coordinate itself depends on wavenumber, rendering it an impracticable vertical coordinate.

in Figs. 3d–f. The CTS term $\mathscr{H}^{\mathrm{CTS}}$ now indeed maximizes very near $\tau = 1$. The basic reason for this is that by Eq. (11), $d\tau/dp = \beta\tau/p$ and thus $\mathscr{H}^{\mathrm{CTS}}$ can be written

$$\mathscr{H}^{\mathrm{CTS}} = -\frac{g}{C_p} B \frac{\beta}{p} \tau e^{-\tau}. \tag{19}$$

The factor $\tau e^{-\tau}$ maximizes at $\tau = 1$, yielding the $\tau = 1$ law. (Of course, B and $1/p$ in Eq. (19) will also vary in the vertical, causing slight deviations from the $\tau = 1$ law as visible in Figs. 3d–f. These deviations are typically small, however, as shown in appendix B). The extra factor of τ in Eq. (19) relative to Eq. (1b) is thus critical, and arises because $d\tau/dp \sim \tau$. A $\tau = 1$ law then also holds for any other vertical coordinate ξ for which $d\tau/d\xi \sim \tau$, such as $\xi = z$ where a common parameterization is $\tau = \tau_s \exp(-z/H)$ (e.g., Huang and Shahabadi 2014; Weaver and Ramanathan 1995; Held 1982). Physically, the $\tau = 1$ law holds for such coordinates because $\tau \approx 1$ is a "sweet spot," in between $\tau \ll 1$ (where the optical depth gradient $d\tau/d\xi$ goes to 0) and $\tau \ll 1$ (where the transmissivity $e^{-\tau}$ goes to 0). For a coordinate such as $\xi = \tau$, on the other hand, $d\tau/d\xi \nsim \tau$ but rather equals 1 everywhere. The CTS term thus does not maximize at $\tau = 1$, instead continuing to increase as τ decreases below 1, as seen in Figs. 3b,c. [A maximum is eventually reached in these panels, but this is due to a rapid decrease in B as $\tau \to 0$, cf. Eq. (13)]. Thus, the $\tau = 1$ law is not iron-clad, but depends on the choice of vertical coordinate.

In addition to the emergence of a $\tau = 1$ maximum, another consequence of the pressure coordinates used in Figs. 3d–f is the relative enhancement of the exchange terms near the surface, as compared to the $\partial_\tau F$ profiles in Figs. 3a–c. This is again due to the factor of $d\tau/dp \sim \tau$, which is enhanced near the surface when $\tau_s \gg 1$. This surface enhancement of radiative cooling in pressure coordinates reveals a limitation of both the CTS approximation, as well as our criteria in Eqs. (6) and (17): even when the CTS term dominates near $\tau = 1$, near the surface the CTS term will be suppressed by $e^{-\tau_s}$ and will typically be much *smaller* than AX and GX there (this effect is not captured by the scalings (5) because these scalings ignored this exponential transmissivity factor). In RCE with $\gamma \ll 1$ and in τ coordinates this failure of the CTS approximation is hidden as *all* terms are small near the surface, compared to the value of the CTS term at $\tau = 1$ (Fig. 3c). In p coordinates, however, the surface enhancement of radiative cooling brings this failure of the CTS approximation to light (Fig. 3f). This breakdown of the CTS approximation for heating rates near the surface was noted earlier by Joseph et al. (1976), and will also be evident in the more realistic heating rates we compute in the next section.

6. Application to real greenhouse gases

The results so far have only been for idealized gray gases obeying the simple relationships (11) and (12). In this section we perform line-by-line radiative transfer calculations for H_2O and CO_2 to test the validity of our results for realistic greenhouse gases. In this section we will use pressure coordinates and apply our decomposition (4) to spectrally resolved heating rates $\mathscr{H}_{\tilde{\nu}}$, which depend on wavenumber $\tilde{\nu}$ (units of cm^{-1}) and will be plotted in units of $\mathrm{K\,day^{-1}\,cm^{-1}}$.

a. *RFM configuration*

We perform line-by-line calculations using the Reference Forward Model (RFM; Dudhia 2017). These calculations are a subset of those performed in Jeevanjee and Fueglistaler (2020), but for convenience we repeat the details of these calculations here. We run RFM for H_2O and CO_2 separately, using HITRAN 2016 spectroscopic data for H_2O from 0 to $1500\,\mathrm{cm^{-1}}$ and CO_2 from 500 to $850\,\mathrm{cm^{-1}}$, using only the most common isotopologue for each gas. We use a highly idealized RCE atmospheric profile with $T_s = 300\,\mathrm{K}$ and a constant lapse rate of $\Gamma = 7\,\mathrm{K\,km^{-1}}$ up to an isothermal stratosphere at 200 K. [Note that the gray RCE temperature profile (10) decreases toward 0 as $p \to 0$, unlike the isothermal stratosphere profile we employ in this section]. The GHG distributions are given by a tropospheric relative humidity of 0.75, a stratospheric H_2O concentration of 23 ppmv (corresponding to an RH of 0.75 at the tropopause, and relatively large due to the 200-K tropopause), and a uniform CO_2 concentration of 280 ppmv. We run RFM at a spectral resolution of $0.1\,\mathrm{cm^{-1}}$ and a uniform vertical resolution of 100 m up to model top at 50 km. RFM's χ factor, following Cousin et al. (1985), is used to suppress far-wing absorption of CO_2. We output optical depth and fluxes as a function of wavenumber and pressure. Profiles of the exchange terms AX and SX were produced by feeding the optical depth profiles from RFM into an offline code which numerically evaluates Eqs. (3) (sanity checks on this calculation are given in Fig. 5). The CTS and GX terms are straightforwardly evaluated from Eqs. (1b) and (1a).

For simplicity in comparing to our offline decomposition, optical depth is calculated along a vertical path (zenith angle of zero), and fluxes were computed using a

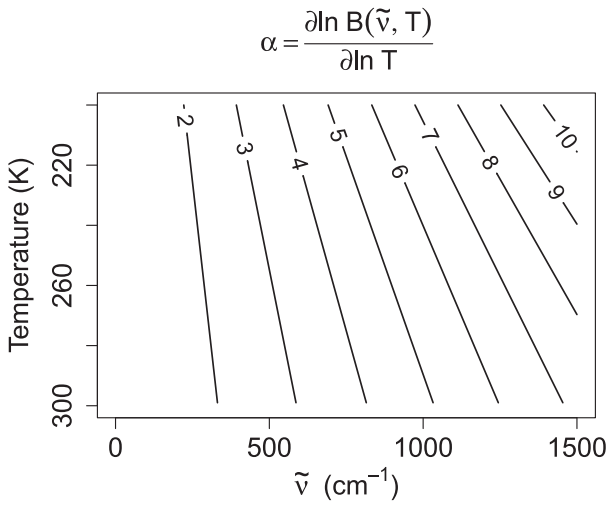

FIG. 4. Contour plot of $\alpha \equiv \partial \ln B(\tilde{\nu}, T)/\partial \ln T$, which appears as an exponent in Eq. (12).

two-stream approximation (rather than RFM's default four-stream) with a diffusivity factor of $D = 1.5$.[4] We also omit the water vapor continuum and do not consider overlap between H_2O and CO_2. These omissions are discussed further in section 7 as well as in the companion paper Jeevanjee and Fueglistaler (2020). Note that the CTS approximation in the presence of continuum effects was examined in Clough et al. (1992).

b. *RFM results*

Before examining the RFM results, let us evaluate the criterion (17) for H_2O and CO_2 in our idealized RCE profiles. To evaluate γ we need to estimate α and β from Eqs. (12) and (11). For α, note that $\alpha = \partial \ln B(\tilde{\nu}, T)/\partial \ln T$ varies with both $\tilde{\nu}$ and T (Fig. 4), but is about 3 near $(\tilde{\nu}, T) = (550\,\mathrm{cm}^{-1}, 260\,\mathrm{K})$, a typical value for the H_2O rotation band (Jeevanjee and Fueglistaler 2020). For $(\tilde{\nu}, T) = (650\,\mathrm{cm}^{-1}, 260\,\mathrm{K})$ near CO_2 band center, α is closer to 4. We thus set $\alpha_{H_2O} = 3$ and $\alpha_{CO_2} = 4$. As for β, a noncondensable, pressure-broadened, well-mixed greenhouse gas such as CO_2 in Earth's atmosphere is well known to have $\beta_{CO_2} = 2$ (Pierrehumbert 2010). For H_2O, Jeevanjee and Fueglistaler (2020) estimated β and found that it varies somewhat in the vertical but has a typical value[5] of $\beta_{H_2O} = 5.5$. Plugging all of this as well as $\Gamma = 7\,\mathrm{K\,km}^{-1}$ into Eq. (14c) yields

$$\begin{aligned} \gamma_{H_2O} &= 0.1, \\ \gamma_{CO_2} &= 0.4. \end{aligned} \tag{20}$$

According to Eq. (17) and Fig. 3, this suggests that the CTS approximation will hold quite well for H_2O, and less so for CO_2 (at least near $\tau = 1$). Indeed, decomposed cooling profiles from our RFM calculations for wavenumbers with $\tau_s \approx 20$ confirm this (Fig. 5), and furthermore resemble the profiles from our gray RCE calculation (Figs. 3e,f).

Of course, Fig. 5 only shows the decomposition (4) for one wavenumber for each gas. To test the robustness of our conclusions, Figs. 6 and 7 show each of the terms in Eq. (4) across the spectrum, as well as their spectral integrals, for H_2O and CO_2, respectively. These plots confirm that for H_2O the exchange terms are small and the CTS approximation is quite accurate, except near the surface. For CO_2, on the other hand, the exchange terms (and the AX term in particular) yield more substantial errors, at the surface and elsewhere. The SX term also provides the well-known tropopause heating from CO_2 (e.g., Thuburn and Craig 2002; Zhu et al. 1992). Physically, the CTS approximation holds well for H_2O because Clausius–Clapeyron scaling of H_2O concentrations yields a fairly rapid increase of τ with p (i.e., large β), and hence a small source function gradient $dB/d\tau$, suppressing the exchange terms.

7. Summary and discussion

We summarize our results as follows:

- We present a new decomposition of radiative flux divergence [Eq. (4)] which better captures the cancellation of exchange terms (Fig. 2).
- We derive the criterion $\gamma \ll 1$ for the validity of the CTS approximation, near $\tau = 1$ and in the case $\tau_s \gg 1$. Exchange terms are suppressed by factors of γ and $1/\tau$ [Eq. (15)], though these terms can manifest near the surface in p coordinates (Fig. 3).
- We find that $\gamma_{H_2O} = 0.1$ and $\gamma_{CO_2} = 0.4$, consistent with the CTS approximation being quite accurate for H_2O but less so for CO_2, at least away from the surface (Figs. 5–7).

These results have been derived in a highly idealized context: our simplified temperature profile has a uniform lapse rate troposphere and isothermal stratosphere, RH is constant, and we have neglected the water vapor continuum as well as H_2O–CO_2

[4] We also disable RFM's BFX flag, and thus assume a constant Planck function $B(\tilde{\nu}, T)$ within vertical grid cells, rather than the linearly varying interpolation which the BFX flag produces.

[5] This is larger than the $\beta = 4$ value for H_2O sometimes found in the literature (e.g., Frierson et al. 2006), likely because those studies neglected pressure broadening in estimating β.

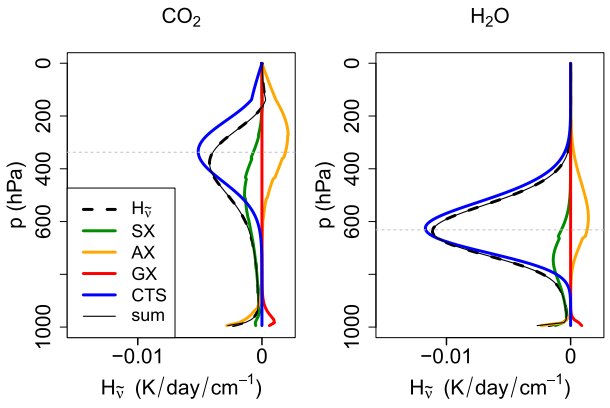

FIG. 5. Spectrally resolved heating rates $\mathscr{H}_{\tilde{\nu}}$ for CO_2 and H_2O, for wavenumbers with $\tau_s \approx 20$ ($\tilde{\nu} = 710\,\mathrm{cm}^{-1}$ and $\tilde{\nu} = 428\,\mathrm{cm}^{-1}$, respectively), decomposed according to Eq. (4). Gray dashed lines show $\tau = 1$ level. These panels bear a resemblance to Figs. 3e and 3f, respectively, and suggest that the CTS approximation works well for H_2O but less so for CO_2. The sum of the terms in Eq. (4) computed offline (thin solid black line) compares very well to the heating calculated by differencing the net flux from RFM (black dashed line).

overlap. Further work should investigate in detail how these assumptions and omissions affect the phenomena considered here and the conclusions given above. In the meantime, we offer a qualitative discussion here.

Let us begin with our simplified temperature profile. Generalizing our results to a nonisothermal stratosphere should be straightforward, as stratospheres with roughly constant lapse rates can also be modeled using Eq. (10). Negative lapse rates typical of the stratosphere will yield $\gamma < 0$ and thus could change the sign of the various exchange terms [cf. Eq. (15)], but we expect that generalizing Eq. (17) to $|\gamma| \ll 1$ would still yield a criterion for the CTS approximation to hold. Furthermore, the small lapse rates typical of the stratosphere should favor the validity of the CTS approximation. For example, for CO_2 in a stratosphere with $\Gamma = -2\,\mathrm{K\,km}^{-1}$, Eq. (14c) yields $\gamma = -0.12$. This seems consistent with the validity of the CTS approximation for stratospheric CO_2 (e.g., Rodgers and Walshaw 1966, their Figs. 2a,c).

At the same time, more realistic temperature profiles can also have strong vertical *gradients* in Γ, arising, for example, at boundary layer or trade inversions, or at the tropopause or stratopause. This will likely lead to strong SX heating/cooling (because this term measures curvature in the temperature profile), and hence to a localized breakdown in the CTS approximation. Such a strong SX contribution can be seen at the tropopause for CO_2 in Fig. 7, and also occurs at the stratopause (e.g., Clough and Iacono 1995; Zhu et al. 1992).

Besides simplified temperature profiles, we also assumed constant RH. Relaxing this would add additional vertical variation to $\beta = d\ln\tau/d\ln p$ for H_2O, but should not affect γ or the CTS approximation in any other way. Other impacts of variable RH, unrelated to the CTS approximation, are discussed in Jeevanjee and Fueglistaler (2020). Convenient cases for studying these effects from more realistic temperature and humidity profiles might be those used in the Continual Intercomparison of Radiation Codes (CIRC; Oreopoulos and Mlawer 2010).

As for continuum absorption from H_2O, this should increase β since $\tau(p)$ for such wavenumbers will depend quadratically on vapor density (because continuum pressure-broadening is largely self-broadening, e.g., Pierrehumbert 2010), and such $\tau(p)$ will thus have an enhanced Clausius–Clapeyron dependence and thus be even more bottom heavy. This larger β would lead to a smaller γ, although it is unclear whether the CTS term would totally dominate at such wavenumbers. This is because such wavenumbers also tend to have $\tau_s \sim O(1)$ (at least in the present-day tropics), and thus the CTS term will overlap with the AX surface cooling already discussed. Also note that absolute values of lower-tropospheric H_2O cooling rates are strongly influenced by the continuum (Jeevanjee and Fueglistaler 2020), a caveat which should be kept in mind when interpreting Fig. 6.

Another influence on the strength of tropospheric cooling rates is H_2O–CO_2 overlap, which we have also neglected. How, then, should our conclusion that the CTS approximation applies well to H_2O, but not as well to CO_2, be applied to Earth's atmosphere which contains both? Evaluation of the CTS approximation, as in Fig. 6f but in the presence of both H_2O and CO_2, shows that while the presence of CO_2 noticeably reduces tropospheric cooling rates, there is no noticeable degradation of the CTS approximation itself relative to the H_2O-only case (not shown). This is because the reduction in tropospheric cooling due to CO_2 is due to a replacement of tropospheric H_2O cooling by largely *stratospheric* CO_2 cooling (which is of course also how CO_2 lowers OLR). The actual contribution of CO_2 to tropospheric cooling is quite small relative to H_2O (cf. Figs. 6f and 7f), so errors in the CTS approximation to this small contribution are negligible.

In addition to studying more realistic cases, future work could also analyze the validity of the CTS approximation for other terrestrial GHGs, such as

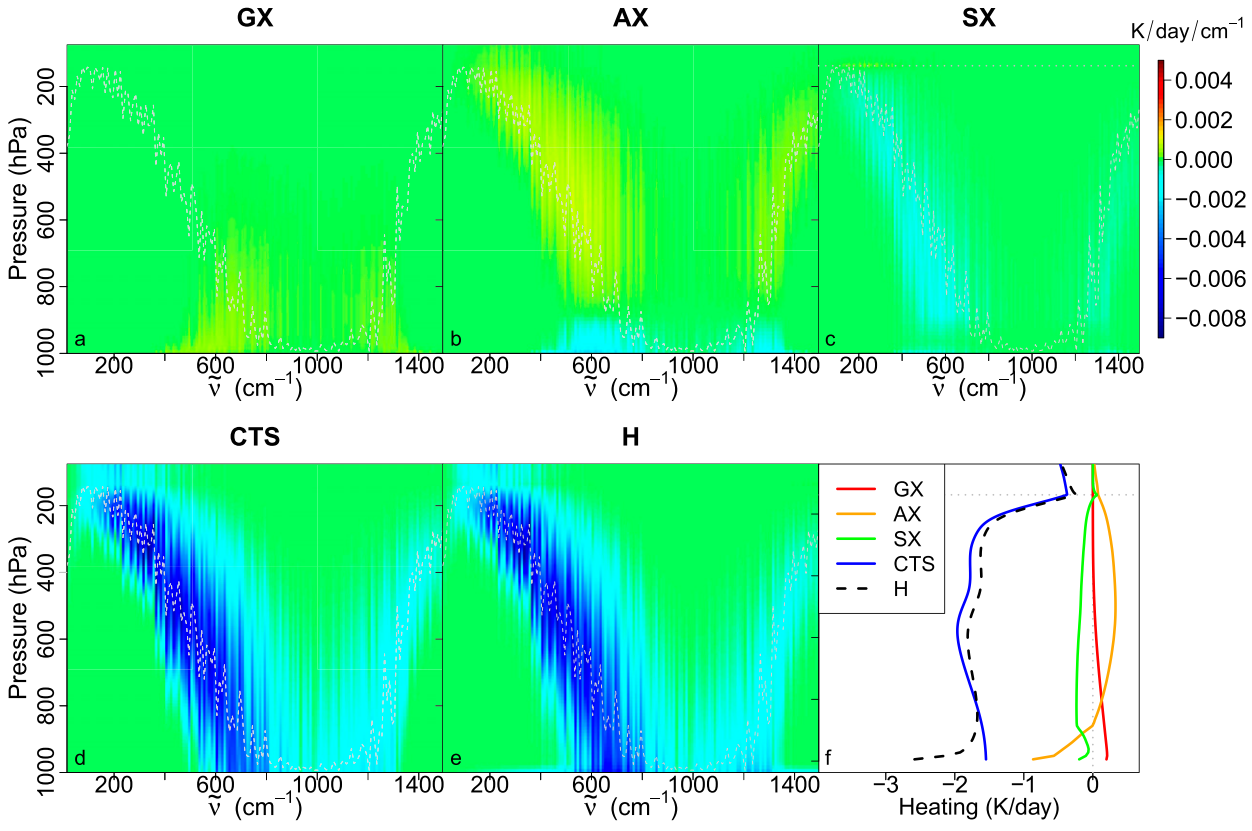

FIG. 6. (a)–(e) The decomposition of $\mathscr{H}_{\tilde{\nu}}$, as in Fig. 5, but now for all wavenumbers $\tilde{\nu}$ and for H_2O only. (f) Corresponding spectral integrals. This figure confirms that for H_2O the CTS approximation is quite accurate and the exchange terms are small, except near the surface. In (a)–(e) averages over spectral bins of width 10 cm^{-1} are shown for clarity (results are not sensitive to this binning). Also shown in (a)–(e) are the $\tau = 1$ contours (gray dashed line), and (c) and (f) show the tropopause height (horizontal gray dotted line).

ozone or methane. Such cases may have different α and β values, and hence different γ. The 1300-cm^{-1} band of methane, for instance, will have α much larger than 3 or 4 (Fig. 4). Furthermore, the parameterization (11) of a gas's vertical distribution may not be appropriate for some gases, as in the case of ozone which is neither well mixed nor bottom heavy.

Going further afield, one might also apply the decomposition (4) to understand and model radiative cooling on other worlds, both within our solar system as well as exoplanets (e.g., Amundsen et al. 2014; Dufresne et al. 2005). If the CTS approximation holds, this might lead to simplified understanding as well as reductions in computational expense, similar to those leveraged in the past for terrestrial radiation (e.g., Schwarzkopf and Fels 1991; Fels and Schwarzkopf 1975).

Acknowledgments. This research was supported by NSF Grants AGS-1417659 and AGS-1660538, and NJ was supported by a Hess fellowship from the Princeton Department of Geosciences. NJ thanks Jacob Seeley and Robert Pincus for helpful feedback and encouragement, as well as Daniel Koll and two anonymous reviewers for very helpful reviews. RFM output and R scripts used in producing this manuscript are available at https://github.com/jeevanje/18cts.git.

APPENDIX A

Analysis of Exchange Terms in RCE

In this appendix we derive Eqs. (16) for the various exchange terms at $\tau \approx 1$ in RCE. For analytic tractability we assume $\tau_s \gg 1$, which then implies $\tau < \tau_s/2$.

We begin with the SX term in Eq. (3a), and Taylor-expand the expression in brackets in Eq. (3a) around $x = 0$ to obtain the diffusive approximation $x^2(d^2B/d\tau^2)$. Note that because of the power-law form of $\tau(p)$, this diffusive approximation only holds for $x \gtrsim 1$ if we have $\tau \gtrsim 1$. With this caveat in mind, we combine the diffusive approximation with Eq. (13) to obtain

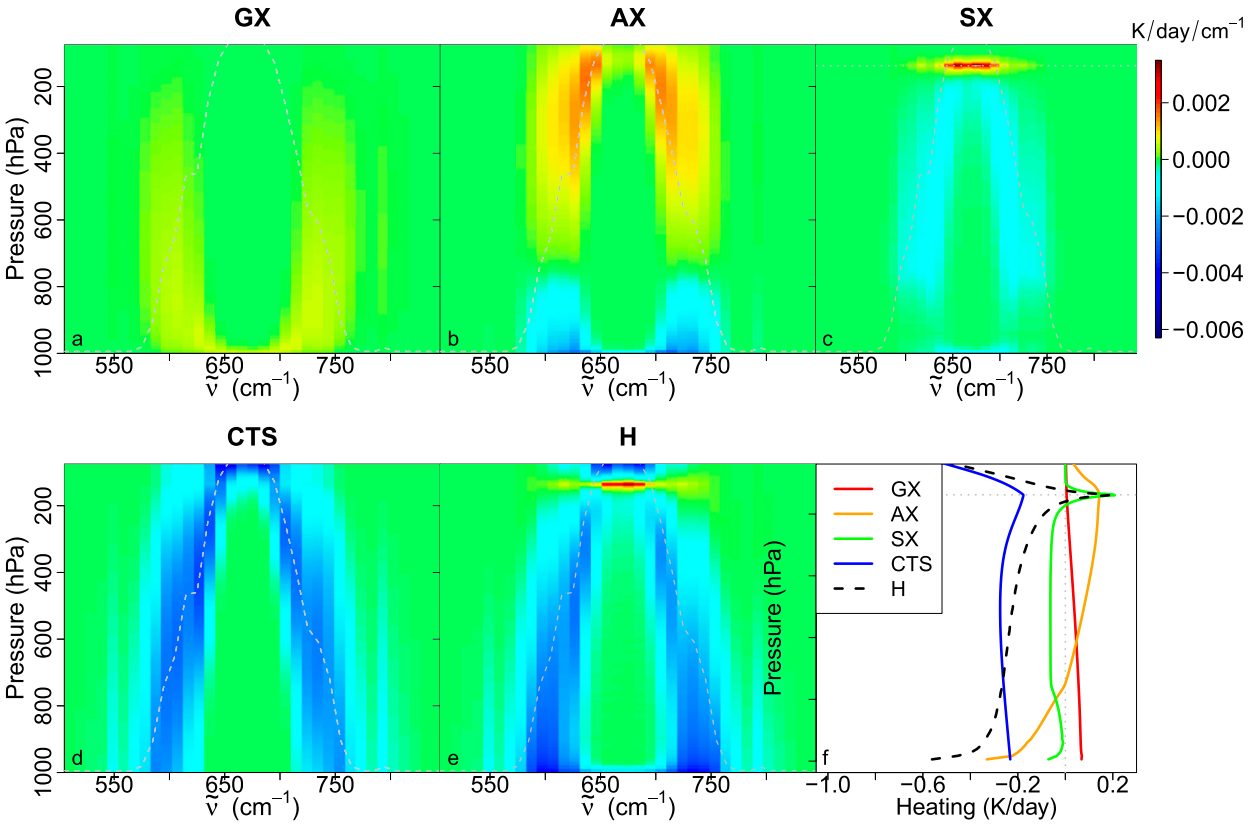

FIG. 7. As in Fig. 6, but for CO_2. The color bar is identical up to an overall scaling. In this case the exchange terms are more significant and the CTS approximation less accurate, as predicted by Eqs. (17) and (20). Note the strong contribution of the SX term at the tropopause (gray dotted line).

$$\mathrm{SX} \approx \frac{\gamma(\gamma-1)B}{\tau^2}\int_0^{\tau} x^2 e^{-x}\,dx. \tag{A1}$$

Note that SX $\to 0$ as $\tau \to 0$ since τ is the thickness of the symmetric layer (Fig. 1). The SX approximation in Eq. (3c) maximizes close to $\tau = 1$ (actually at $\tau \approx 1.45$), where the integral has a value of 1/6.

For AX we similarly Taylor-expand the integrand in Eq. (3b) as $x(dB/d\tau)$ (again only trusting this approximation for $\tau \gtrsim 1$):

$$\begin{aligned}\mathrm{AX} &\approx \frac{\gamma B}{\tau}\int_{\tau}^{\tau_s-\tau} x e^{-x}\,dx \\ &\approx \gamma\frac{\tau+1}{\tau}Be^{-\tau}.\end{aligned} \tag{A2}$$

For GX we similarly approximate $B(\tau_s) - B(\tau)$ as $dB/d\tau(\tau_s - \tau)$ and thus obtain

$$\mathrm{GX} = \frac{\gamma B}{\tau}(\tau_s-\tau)e^{-(\tau_s-\tau)}. \tag{A3}$$

Note that SX, AX, and GX in Eqs. (A1)–(A3) indeed resemble the scalings (15), though with additional structure [also bear in mind that Eq. (A2) only holds for $\tau < \tau_s/2$]. Evaluating Eqs. (A1)–(A3) as well as Eq. (1b) at $\tau = 1$, and noting that $xe^{-x} \le 1/e$, then yields Eqs. (16) in the main text.

APPENDIX B

Further Analysis of the $\tau = 1$ Law

In this appendix we further analyze the $\tau = 1$ law in pressure coordinates. This law can be applied to both the maximum in $\mathscr{H}^{\mathrm{CTS}}$ discussed in section 5 [Eq. (19)], as well as the maximum in the transmissivity gradient or "weighting function"

$$W \equiv -\frac{d(e^{-\tau})}{dp} \tag{B1}$$

(e.g., Wallace and Hobbs 2006; Petty 2006). We will address both of these applications in turn.

We begin by studying the maximum of W, as the top-of-atmosphere flux $F(\tau = 0) = -\int_0^{p_s} B(p)[d(e^{-\tau})/dp]\,dp$ is a convolution of W with the source function profile, and

thus the location of the W maximum serves as an effective "emission level" for $F(\tau = 0)$. Substituting Eq. (11) into Eq. (B1) and differentiating shows that W maximizes at

$$\tau_{\max,W} = 1 - \frac{1}{\beta}. \tag{B2}$$

Since $\beta \geq 2$ in general, this shows that $1/2 \leq \tau_{\max,W} < 1$. For H_2O with $\beta = 5.5$, $\tau_{\max,W} \approx 0.8$, fairly close to one. For CO_2 with $\beta = 1/2$, however, we find $\tau_{\max,W} = 1/2$, so nonnegligible deviations from the $\tau = 1$ law for W are possible.

Now we turn to the maximum in $\mathscr{H}^{\mathrm{CTS}}$, which (up to constants) is simply W multiplied by the source function B. In section 5 we argued that the vertical structure of this term is dominated by the $\tau e^{-\tau}$ factor in Eq. (19). To justify this, we differentiate Eq. (19) and find that $\mathscr{H}^{\mathrm{CTS}}$ maximizes at

$$\tau_{\max,\mathscr{H}} = 1 - \frac{1}{\beta} + \gamma. \tag{B3}$$

Note the similarity to Eq. (B2). The "1" on the right-hand side of Eq. (B3) comes from the $\tau e^{-\tau}$ factor, the $1/\beta$ comes from β/p, and the γ comes from B, using Eq. (13). Note that the latter two effects have opposite signs in the troposphere, so the $\tau = 1$ law there should indeed hold better for $\mathscr{H}^{\mathrm{CTS}}$ than for W.

To evaluate Eq. (B3), we note that β and γ are related by Eq. (14c) and we thus rewrite Eq. (B3) as

$$\tau_{\max,\mathscr{H}} = 1 - \frac{1}{\beta}\left(1 - \frac{\alpha R_d \Gamma}{g}\right). \tag{B4}$$

For CO_2 in RCE with $\alpha = 4$, $\beta = 2$, and $\Gamma = 7\,\mathrm{K\,km^{-1}}$, this gives $\tau_{\max,\mathscr{H}} = 0.91$, very close to 1. A similar value is obtained for H_2O with $\alpha = 3$ and $\beta = 5.5$. While Eq. (B4) can in principle yield values far from 1, this seems to require combinations of the parameters α, β, and Γ which are unrealistic or irrelevant, at least for H_2O and CO_2 on Earth. The only relevant case we have found is that of a stratosphere with negative lapse rate, for example, $\Gamma = -2\,\mathrm{K\,km^{-1}}$, in which case $\tau_{\max,\mathscr{H}} = 0.38$ for CO_2. We do not consider other GHGs (e.g., ozone, methane) or other worlds, however, for which these conclusions may differ.

REFERENCES

Amundsen, D. S., I. Baraffe, P. Tremblin, J. Manners, W. Hayek, N. J. Mayne, and D. M. Acreman, 2014: Accuracy tests of radiation schemes used in hot Jupiter global circulation models. *Astron. Astrophys.*, **564**, A59, https://doi.org/10.1051/0004-6361/201323169.

Andrews, D. G., C. B. Leovy, J. R. Holton, J. Marshall, and R. A. Plumb, 1987: *Middle Atmosphere Dynamics*. Elsevier, 502 pp.

Clough, S. A., and M. J. Iacono, 1995: Line-by-line calculation of atmospheric fluxes and cooling rates: 2. Application to carbon dioxide, ozone, methane, nitrous oxide and the halocarbons. *J. Geophys. Res.*, **100**, 16 519–16 535, https://doi.org/10.1029/95JD01386.

——, ——, and J.-l. Moncet, 1992: Line-by-line calculations of atmospheric fluxes and cooling rates: Application to water vapor. *J. Geophys. Res.*, **97**, 15 761–15 785, https://doi.org/10.1029/92JD01419.

Cousin, C., R. L. Doucen, C. Boulet, and A. Henry, 1985: Temperature dependence of the absorption in the region beyond the 4.3-μm band head of CO_2. 2: N_2 and O_2 broadening. *Appl. Opt.*, **24**, 3899–3907, https://doi.org/10.1364/AO.24.003899.

Cronin, T. W., and M. F. Jansen, 2016: Analytic radiative-advective equilibrium as a model for high-latitude climate. *Geophys. Res. Lett.*, **43**, 449–457, https://doi.org/10.1002/2015GL067172.

Dudhia, A., 2017: The Reference Forward Model (RFM). *J. Quant. Spectrosc. Radiat. Transf.*, **186**, 243–253, https://doi.org/10.1016/j.jqsrt.2016.06.018.

Dufresne, J., R. Fournier, C. Hourdin, and F. Hourdin, 2005: Net exchange reformulation of radiative transfer in the CO_2 15-μm band on Mars. *J. Atmos. Sci.*, **62**, 3303–3319, https://doi.org/10.1175/JAS3537.1.

Eymet, V., J. L. Dufresne, P. Ricchiazzi, R. Fournier, and S. Blanco, 2004: Long-wave radiative analysis of cloudy scattering atmospheres using a net exchange formulation. *Atmos. Res.*, **72**, 239–261, https://doi.org/10.1016/j.atmosres.2004.03.017.

Fels, S. B., and M. D. Schwarzkopf, 1975: The simplified exchange approximation: A new method for radiative transfer calculations. *J. Atmos. Sci.*, **32**, 1475–1488, https://doi.org/10.1175/1520-0469(1975)032<1475:TSEAAN>2.0.CO;2.

Frierson, D. M. W., I. M. Held, and P. Zurita-Gotor, 2006: A gray-radiation aquaplanet moist GCM. Part I: Static stability and eddy scale. *J. Atmos. Sci.*, **63**, 2548–2566, https://doi.org/10.1175/JAS3753.1.

Goody, R. M., and Y. L. Yung, 1989: *Atmospheric Radiation: Theoretical Basis*. 2nd ed. Oxford University Press, 544 pp.

Green, J. S., 1967: Division of radiative streams into internal transfer and cooling to space. *Quart. J. Roy. Meteor. Soc.*, **93**, 371–372, https://doi.org/10.1002/qj.49709339710.

Held, I. M., 1982: On the height of the tropopause and the static stability of the troposphere. *J. Atmos. Sci.*, **39**, 412–417, https://doi.org/10.1175/1520-0469(1982)039<0412:OTHOTT>2.0.CO;2.

Huang, Y., and M. B. Shahabadi, 2014: Why logarithmic? A note on the dependence of radiative forcing on gas concentration. *J. Geophys. Res.*, **119**, 13 683–13 689, https://doi.org/10.1002/2014JD022466.

Jeevanjee, N., and D. M. Romps, 2018: Mean precipitation change from a deepening troposphere. *Proc. Natl. Acad. Sci. USA*, **115**, 11 465–11 470, https://doi.org/10.1073/pnas.1720683115.

——, and S. Fueglistaler, 2020: Simple spectral models for atmospheric radiative cooling. *J. Atmos. Sci.*, **77**, 479–497, https://doi.org/10.1175/JAS-D-18-0347.1.

Joseph, J. M., R. Bursztyn, J. M. Joseph, and R. Bursztyn, 1976: A radiative cooling model in the thermal infrared for application to models of the general circulation. *J. Appl. Meteor.*, **15**, 319–325, https://doi.org/10.1175/1520-0450(1976)015<0319:ARCMIT>2.0.CO;2.

Oreopoulos, L., and E. Mlawer, 2010: The Continual Intercomparison of Radiation Codes (CIRC). *Bull. Amer. Meteor. Soc.*, **91**, 305–310, https://doi.org/10.1175/2009BAMS2732.1.

Petty, G. W., 2006: *A First Course in Atmospheric Radiation*. 2nd ed. Sundog Publishing, 472 pp.

Pierrehumbert, R. T., 2010: *Principles of Planetary Climate*. Cambridge University Press, 674 pp.

Robinson, T. D., and D. C. Catling, 2012: An analytic radiative-convective model For planetary atmospheres. *Astrophys. J.*, **757**, 104, https://doi.org/10.1088/0004-637X/757/1/104.

Rodgers, C. D., and C. D. Walshaw, 1966: The computation of infrared cooling rate in planetary atmospheres. *Quart. J. Roy. Meteor. Soc.*, **92**, 67–92, https://doi.org/10.1002/qj.49709239107.

Schwarzkopf, M. D., and S. B. Fels, 1991: The simplified exchange method revisited: An accurate, rapid method for computation of infrared cooling rates and fluxes. *J. Geophys. Res.*, **96**, 9075–9096, https://doi.org/10.1029/89JD01598.

Thomas, G. E., and K. Stamnes, 2002: *Radiative Transfer in the Atmosphere and Ocean*. Cambridge University Press, 517 pp.

Thuburn, J., and G. C. Craig, 2002: On the temperature structure of the tropical substratosphere. *J. Geophys. Res.*, **107**, 4017, https://doi.org/10.1029/2001JD000448.

Wallace, J. M., and P. V. Hobbs, 2006: *Atmospheric Science: An Introductory Survey*. Academic Press, 504 pp.

Weaver, C., and V. Ramanathan, 1995: Deductions from a simple climate model: Factors governing surface temperature and atmospheric thermal structure. *J. Geophys. Res.*, **100**, 11 585–11 591, https://doi.org/10.1029/95JD00770.

Zhu, X., M. E. Summers, and D. F. Strobel, 1992: Calculation of CO2 15-μm band atmospheric cooling rates by Curtis matrix interpolation of correlated-k coefficients. *J. Geophys. Res.*, **97**, 12 787–12 797, https://doi.org/10.1029/92JD01311.